GRAVITY WAVE STATISTICS FOR MY34 AND MY35 FROM THE ACS/TGO MEASUREMENTS

E. D. Starichenko, *Space Research Institute of the Russian Academy of Sciences (IKI), Moscow, Russia (starichenko.ed@phystech.edu)*, **A. S. Medvedev**, *Max Planck Institute for Solar System Research, Göttingen, Germany*, **D. A. Belyaev, A. A. Fedorova, O. I. Korablev, A. Trokhimovskiy**, *Space Research Institute of the Russian Academy of Sciences (IKI), Moscow, Russia*, **F. Montmessin**, *LATMOS/IPSL, UVSQ Université Paris-Saclay, UPMC Univ. Paris 06, CNRS, Guyancourt, France*

Introduction:

Gravity waves (GWs) are omnipresent in planetary atmospheres and originate from displacements of air parcels. Since they re-distribute energy and momentum between atmospheric layers, GWs greatly impact atmospheric dynamics. In this work, we study the activity of GWs in the Martian atmosphere from solar occultation experiments conducted by the infrared spectrometers of Atmospheric Chemistry Suite (ACS) (Korablev et al., 2018) on board the Trace Gas Orbiter (TGO).

Observations:

ACS is a part of the TGO, which represents the ESA-Roscosmos ExoMars 2016 collaborative mission. The instrument consists of three infrared channels (Korablev et al., 2018): near-IR (NIR, 0.73-1.6 μm) , middle-IR (MIR, 2.3-4.2 μm) , and thermal-IR (TIRVIM, 1.7-17 μm). In this work, we use the data obtained from the MIR and NIR instruments, operating in solar occultation mode since April 2018. ACS-MIR is a cross-dispersion echelle spectrometer that allows for retrieving temperature and density vertical profiles in the strong 2.7 μm CO_2 absorption band covering the broad altitude range of 20-180 km (Belyaev et al., 2021, 2022). ACS-NIR, an echelle spectrometer combined with an acousto-optic tunable filter, measures the atmospheric structure in the 1.57 μm CO_2 band at altitudes from 10 to 100 km (Fedorova et al., 2020, 2022). Both ACS channels possess a high resolving power, exceeding ~25000, signal to noise ratio more than 1000, and sound the atmosphere with the vertical resolution of 0.5-2.5 km. During simultaneous occultations, the instruments lines of sight target identical tangent points that provide confidential cross validation between the retrieved atmospheric profiles. Presently, we report the observations for 1.5 Martian years (MY), from the middle of MY34 (April 2018) to the end of MY35 (January 2021), counting ~600 occultations of MIR and ~6200 occultations of NIR. Figures 1 and 2 show MIR and NIR data coverages respectively.
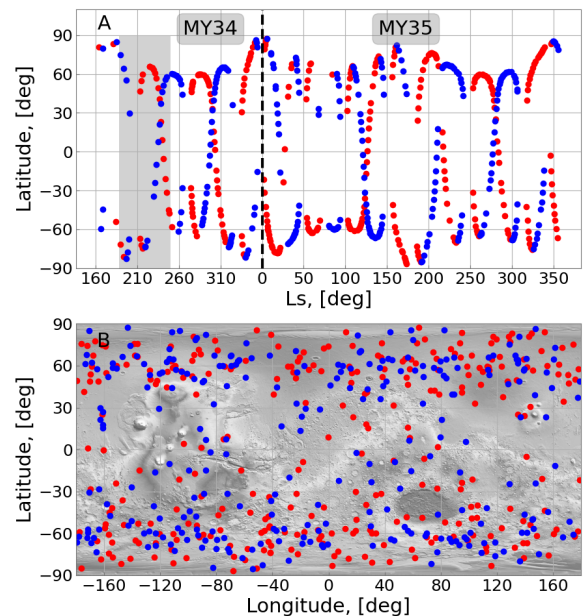

Figure 1: Latitudinal coverage of ACS-MIR occultations versus Solar longitude (Ls) (a) and Martian longitude (b). Grey area in (a) depicts the global dust storm (GDS) period in MY34.
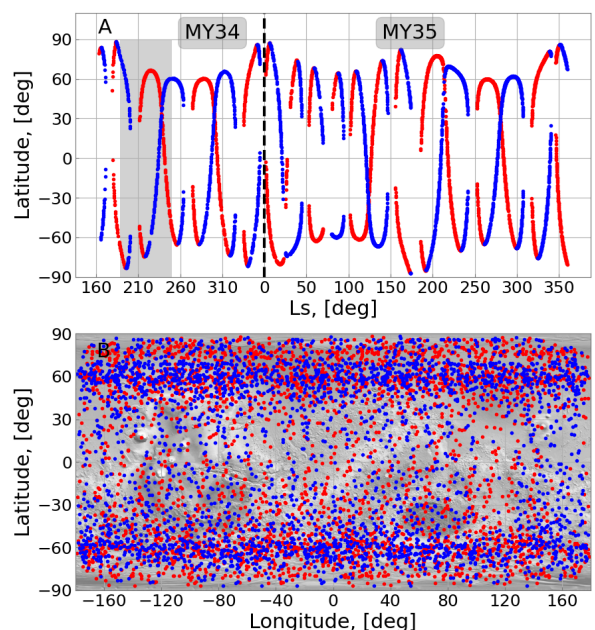

Figure 2: The same as in Fig. 1 but for ACS-NIR.

Results:

In order to derive the parameters of GWs, we use the method described in (Starichenko et al., 2021). Some of these parameters are shown in Figure 3. First, from the vertical temperature profile (Figure 3a, solid black line) we reveal the background temperature profile (Figure 3a, red dashed line). From these two, we find their difference T' and the amplitude (envelope of T') of GW packets (Figure 3b, solid black and red dashed lines respectively). Then we calculate the Brunt-Väisälä frequency, vertical flux of horizontal momentum and acceleration by GWs (Figure 3c,d). Also, we find GW potential energy, which we use as a measure of GW activity in this study.

In many cases we observe the mechanism of GW saturation and breaking (Figure 3b), where the wave amplitude increases with altitude and stops growing at ~110 km. At the same altitude, the Brunt-Väisälä frequency of the net temperature tends to zero (Figure 3c), which means that the temperature gradient is approaching the adiabatic lapse rate, and dissipation process takes place. This process, when the GW transfers its energy to the ambient flow, can be seen in the behavior of the momentum flux profile, which has steep drops, and an increase of acceleration (see Figure 3d).

Figure 4 shows the latitude-altitude distributions of GW amplitude, potential energy, momentum flux and GW drag. The cross-sections obtained from the ACS-MIR data were averaged over the period of MY34. It is seen that amplitudes of temperature fluctuations grow with height. The latitudinal structure of the GW activity in the atmosphere is not uniform. For comparison, the zonal wind distribution simulated with the Max Planck Institute (MAOAM) MGCM (https://mars.mipt.ru/) is depicted with the contour lines. During the time of observation, wind distribution has changed from equinoctial to solstitial and back to equinoctial. The result reflects the largest contribution of the prograde and retrograde jets during the perihelion solstice. The regions with peak values of all depicted characteristics encircle the upper edges of two midlatitude jets. This is the consequence of intense filtering of individual harmonics by strong background winds. This pattern is present in amplitude distribution and is also obvious in other GW parameters, because they are the quadratic functions of amplitude.

Figure 5 is a summary of GW's observations by ACS-MIR for the second halves of MY34 and 35. It is seen that the GW activity is highly intermittent depending on altitude and on season. One can also observe the difference between hemispheres during the perihelion season. GW activity is larger in the northern winter than in the southern summer.

Figure 6 presents seasonal variations of the zonal mean temperature in MY35 observed by the NIR channel. The presented Ls intervals were chosen to encompass maximal local time difference between the morning and evening observations, i.e. ~12h. The temperature for the specified interval of longitudes was computed as the average of all background temperature profiles pertaining to this interval. The difference between morning and evening measurements (Figure 6c) shows big structured contrasts that reflect diurnal tidal fluctuations.
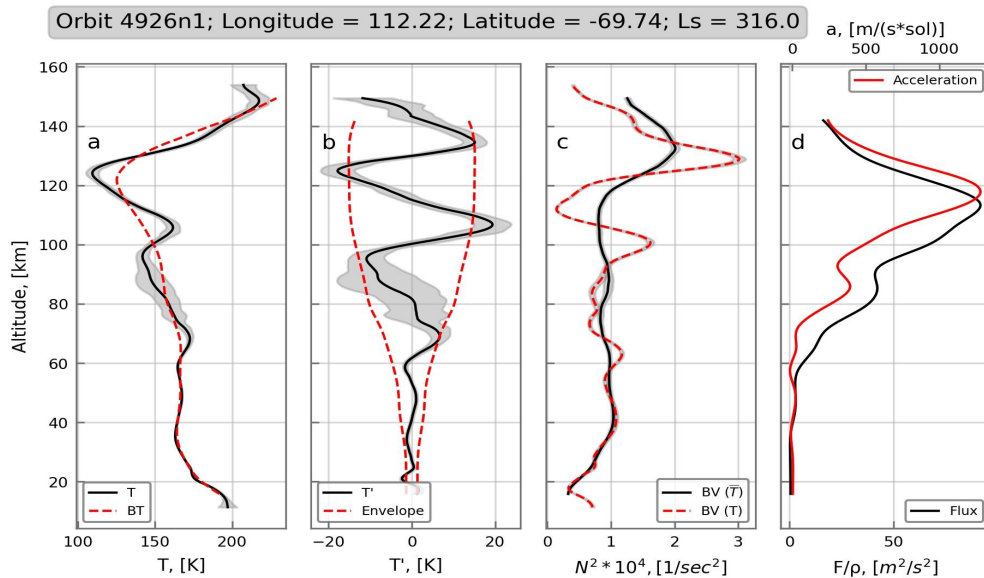

Figure 3: Vertical profiles for the orbit 4926n1: a) The measured (solid black) and fitted mean temperature (red dashed); b) wave temperature disturbance (solid black) and envelope (red dashed); c) Brunt-Väisälä frequency calculated for the mean (black) and net temperature (red dashed); d) momentum flux (black) and mean flow acceleration ("wave drag", upper axis, red). Shading denotes observational uncertainties.
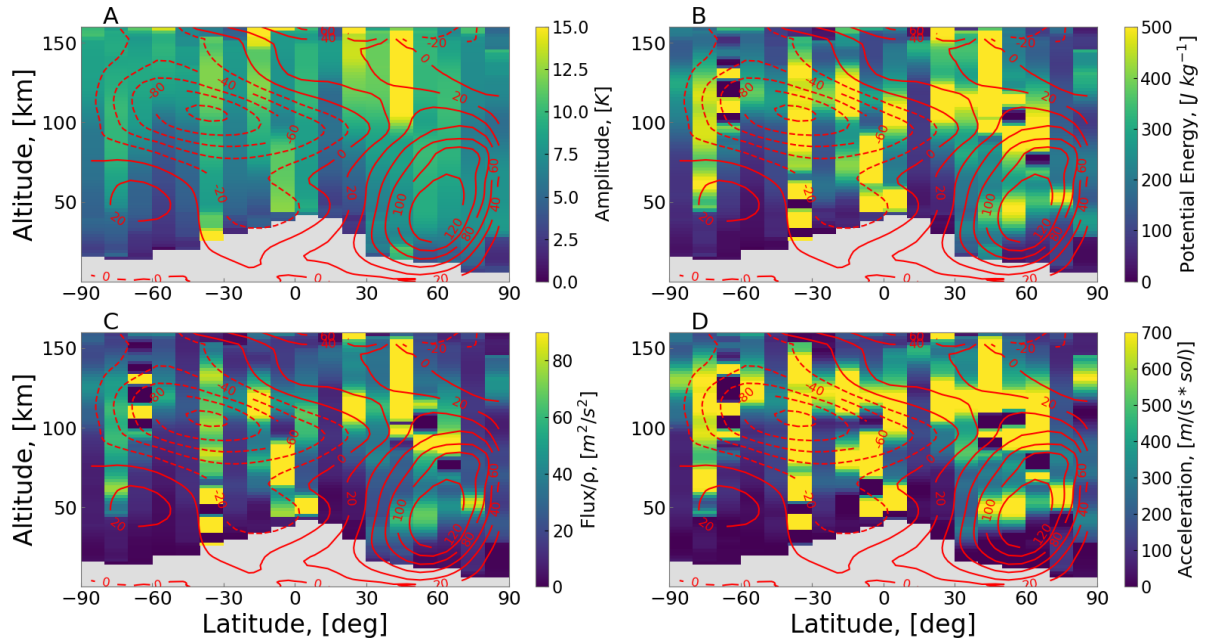
Figure 4: MY34 latitude-altitude cross-sections of the retrieved GW a) amplitudes (in K), b) potential energy (per unit mass), c) vertical fluxes of absolute horizontal momentum (per unit mass) and d) associated momentum forcing (GW drag). The size of the employed latitudinal bins is 10 deg. Contour lines present the zonal wind (in m/s) simulated with the MAOAM MGCM for MY34 (https://mars.mipt.ru/data.php) and averaged over the same as in Figure 4 period of observations.
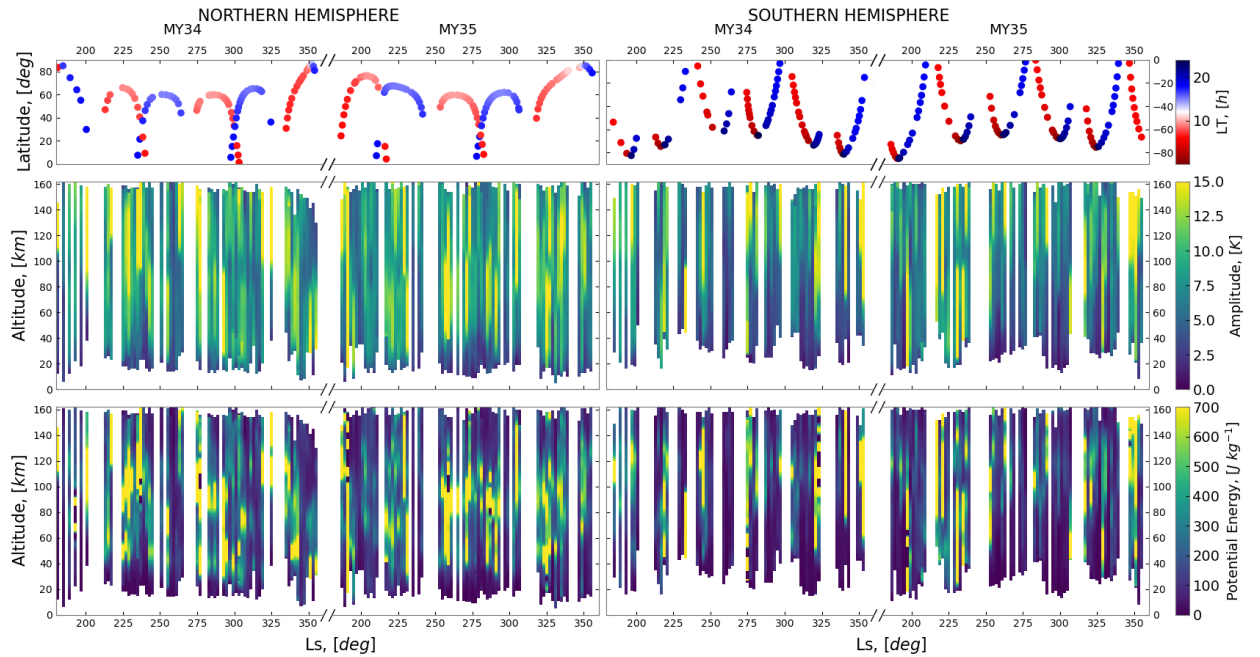

Figure 5: First row: Ls-latitude distribution of ACS-MIR occultations (color depicts morning/evening observations); Second and Third rows: Seasonal-altitude variations of amplitude (in K) and potential energy (per unit mass) for the second parts of MY34 and MY35. Two columns represent northern and southern hemispheres respectively.
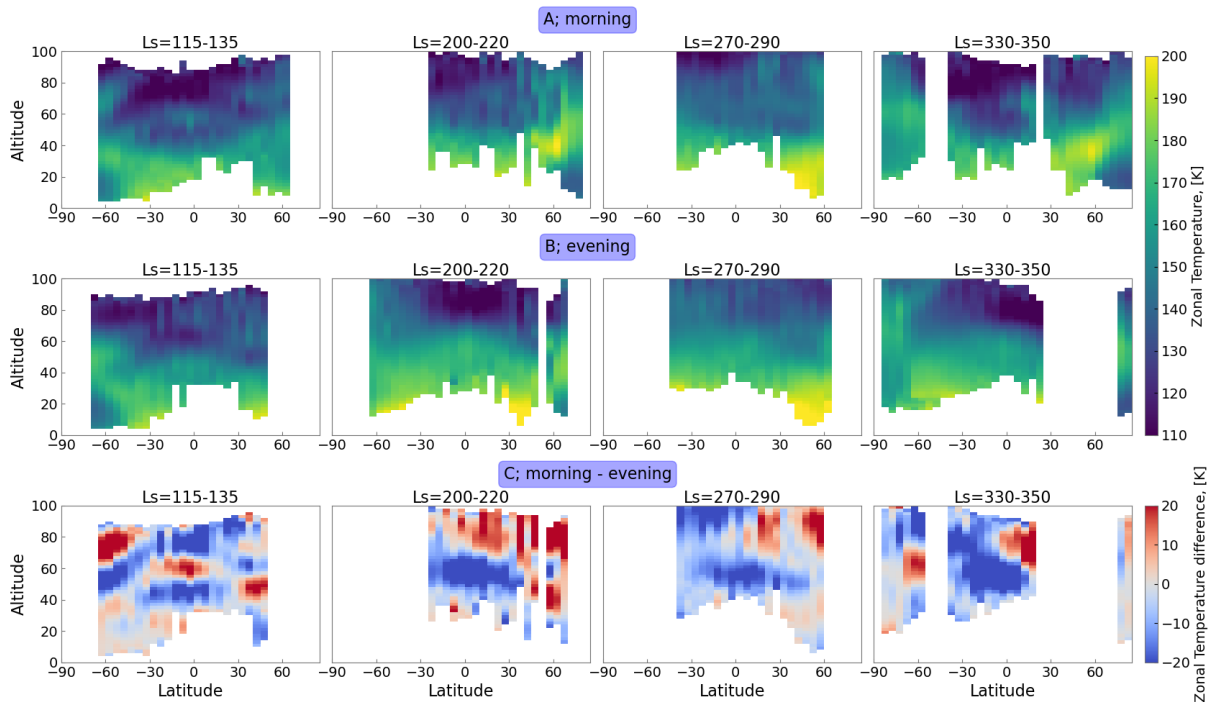
Figure 6: Latitude-altitude cross-sections of the zonal temperatures from the ACS-NIR data averaged over four Ls intervals in MY35. First row: morning (0-12h) observations; Second row: evening (12-24h) observations; Third row: their difference.

Conclusions:

Although small-scale gravity waves represent a major dynamical mechanism in the Martian atmosphere, their statistics remain largely unquantified. The presented ACS measurements for the first time cover almost the entire atmosphere from the troposphere to the middle thermosphere (~160 km) with the vertical resolution sufficient for deriving GW characteristics. The analysis provides evidence of systematic seasonal and intraday variations of the GW activity, whose physical mechanism is to be studied in detail nowadays.

References:

Belyaev D. et al., 2021. Revealing a high water abundance in the upper mesosphere of Mars with ACS onboard TGO. Geophysical Research Letters, 48, e2021GL093411. DOI: 10.1029/2021GL093411

Belyaev D. et al., 2022. Thermal Structure of the Middle and Upper Atmosphere of Mars from ACS/TGO CO2 Spectroscopy. Submitted to Journal of Geophysical Research: Planets. Under Review.

Fedorova A. et al., 2020. Stormy water on Mars: The distribution and saturation of atmospheric water during the dusty season. Science, eaay9522. DOI: 10.1126/science.aay9522.

Fedorova A. et al., 2022. A two-Martian year survey of the water vapor saturation state on Mars based on ACS NIR/TGO occultations. Submitted to Journal of Geophysical Research: Planets.

Korablev O., Montmessin F., and ACS Team, 2018. The Atmospheric Chemistry Suite (ACS) of three spectrometers for the ExoMars 2016 Trace Gas Orbiter. Space Sci. Rev., 214:7. DOI 10.1007/s11214-017-0437-6.

Starichenko E. et al., 2021. Gravity wave activity in the Martian atmosphere at altitudes 20–160 km from ACS/TGO occultation measurements. Journal of Geophysical Research: Planets, 126, e2021JE006899. DOI: 10.1029/2021JE00689